Modeling the effect of turbulence on the simultaneous propagation of multiple parallel hydraulic fractures

Peirce, A.P. [1] and Dontsov, E.V. [2]

[1]*University of British Columbia, Vancouver, BC, Canada*
[2]*University of Houston, Houston, TX, USA*

ABSTRACT: The injection of slick-water at the high rates used to fracture unconventional shale-gas reservoirs results in flows that are turbulent - particularly near the wellbore. In this paper we consider the effect of turbulence on the simultaneous propagation of multiple hydraulic fractures that are constrained to evolve in parallel planes. The effect of turbulence is captured using a modification of the Darcy-Weisbach fluid-flow model with an adaptation of Churchill's friction factor approximation to fracture flow geometries that is able to capture the transition from laminar to fully turbulent flow. Since the Reynolds number is proportional to the fracture width, the flow transitions to laminar close to the tip where the fracture width approaches zero. The model used in this paper is therefore able to exploit the multi-scale laminar tip asymptotic behaviour in order to use the Implicit Level Set Scheme (ILSA) to locate the fracture free boundary and to identify the propagation regime. We provide a numerical example for an array of five uniformly distributed planar fractures in which the laminar model exhibits significant stress shadowing while the turbulent model predicts substantially less. This reduction in stress shadowing in the turbulent flow model is due to the significantly larger pressure drop near the well-bore compared to the laminar case that dominates the mutual stress interactions between the fractures in the array.

1. INTRODUCTION

Hydraulic fractures are tensile fractures induced in a rock formation by the injection of a pressurized fluid. This technique is used to stimulate oil and gas wells Economides and Nolte (2000), for waste disposal Abou-Sayed et al. (1989), to enhance rock mining Jeffrey and Mills (2000), for CO_2 sequestration, and for geothermal energy extraction Brown (2000). To increase the treatment efficiency in unconventional tight-gas reservoirs multiple hydraulic fractures from different perforations are often generated simultaneously from one wellbore. In this situation, outer fractures induce additional compressive stresses on inner fractures and cause non-uniform fracture growth. This phenomenon is called stress shadowing and has been addressed in numerous studies Olson (2008); Singh and Miskimins (2010); McClure and Zoback (2013); Kresse et al. (2013); Peirce and Bunger (2014); Daneshy (2014); Wu et al. (2015); Skomorowski et al. (2015); Kumar and Ghassemi (2015); Manchanda et al. (2016); Dontsov and Peirce (2016) and can significantly affect the fracture geometry and the associated production rate. For this reason, it is important to develop numerical models that are able to predict simultaneous growth of multiple hydraulic fractures and that can be used to design more efficient hydraulic fracture stimulations.

The past decade has seen a shift from the use of high viscosity cross-linked gels in conventional hydraulic fracture treatments to the deployment of slick-water driven hydraulic fractures at high injection rates in the stimulation of impermeable shale gas deposits. For the conventional, high viscosity, moderate-injection treatments the modeling assumption of a predominantly laminar flow within the fracture has been used to good effect. However, for typical treatments in unconventional reservoirs the viscosity decrease of the water-based injection fluids and the increased injection rates result in flows within the fracture for which the Reynolds numbers, particularly near the wellbore, are in the turbulent regime. At the same time, the Reynolds number is proportional to the fracture width, which implies that there is always a region near the fracture tip where the flow is laminar. It is therefore important to use a model that is able to capture the laminar flow, the turbulent flow, and the laminar-to-turbulent transition.

In this paper we explore the effect of the turbulence associated with these high Reynolds numbers on the simultaneous propagation of multiple hydraulic fractures in distinct parallel planes. The turbulence model uses the approximate phenomenological Darcy-Weisbach fluid-flow equation in which Churchill's approximation of the dimensionless friction factor for circular pipes has been adapted to fracture flow geometries, and which is able to capture laminar, laminar-to-turbulent, and turbulent regimes. In the regions near the tip the Reynolds number is assumed to be sufficiently small, due to the reduced fracture width, that the flow is laminar. In this case the tip asymptotic behaviour, established for laminar flows, can still be used to determine the location of the free boundary using the Implicit Level Set Algorithm (ILSA). This algorithm is able to capture multiscale tip asymptotic behaviour that results when multiple physical processes compete to determine the location of the fracture boundary. In the examples considered the evolving fracture footprints for turbulent flows are compared to models in which the flow is assumed to be laminar.

2. MATHEMATICAL MODEL

2.1. ASSUMPTIONS

To formulate the mathematical model to describe the simultaneous growth of multiple parallel hydraulic fractures, it is first necessary to outline a list of assumptions that are used in the model. In particular, it is assumed that:

- All the fractures are planar and perpendicular to the wellbore, see Fig. 1. Five fractures are considered in this paper, but the methodology can be easily extended to any number of fractures.

- Linear elastic fracture mechanics (LEFM) applies for describing the fracture growth, see e.g. Rice (1968).

- The rock is linearly elastic and poroelastic effects are ignored.

- The fluid is assumed to be incompressible and Newtonian with a dynamic viscosity μ. The fluid flow is governed by the Darcy-Weisbach equation in which we use an adaptation to hydraulic fracture geometries of Churchill's approximation of the friction factor (Churchill, 1977) that applies over a wide range of Reynolds numbers.

- The leak-off is described by Carter's model Carter (1957), which assumes a one-dimensional diffusion in the direction perpendicular to the fracture surface, and is quantified by the leak-off coefficient C_L.

- The rock is homogeneous (i.e. the fracture toughness K_{Ic}, Young's modulus E, Poisson's ratio ν, and leak-off coefficient C_L all have uniform values).

- All fractures are always in limit equilibrium, in which case the stress intensity factor is always equal to the fracture toughness at the crack tip.

- The effect of gravity is neglected.

- The fluid front coincides with the crack front, since the lag between the two fronts is negligible under typical high confinement conditions encountered in reservoir stimulation Garagash and Detournay (2000); Detournay and Peirce (2014).

- The effect of perforation friction is not considered.

- The pay zone layer with height H is surrounded by two other layers, in which an additional compressive stress $\Delta\sigma$ is applied, see Fig. 1. Only two symmetric stress barriers are considered in this study for the purpose of numerical examples. The approach can be extended to arbitrary spatial variation of the compressive stresses. Note that the all layers have the same elastic constants. Capturing spatial variation of elastic properties requires substantial modification of the algorithm that is used in this study.

2.2. GOVERNING EQUATIONS

This section outlines the governing equations for multiple parallel hydraulic fractures. With the reference to Fig. 1, it is noted that the z coordinate lies along the wellbore, while each fracture is contained in the (x, y) plane. The source (wellbore) with total volumetric injection rate $Q(t)$ is located at the origin of each (x, y) plane that contains a fracture, i.e. $(0, 0, z_l)$, where z_l is the location of the perforation and $l = 1...n_p$ is the fracture number ($n_p = 5$ is the total number of fractures). In this setting, the primary quantities of interest in a hydraulic fracture problem are the time histories of the fracture displacement discontinuity components $D_{j,l}(x, y, t)$ $j = 1, 2, 3$, the fluid pressure $p_l(x, y, t)$, the fluid flux entering each fracture $Q_l(t)$, and the position of the front $C_l(t)$. Here $l = 1...n_p$, in which case all the above quantities are calculated for each hydraulic fracture. The fracture width is determined from the displacement discontinuity values as $w_l = D_{z,l}(x, y, t)$. The solution depends on the injection rate $Q(t)$, the far-field compressive stress σ_{zz}, (perpendicular to the fracture planes), and four material parameters μ', E', K', and C' defined as

$$
\begin{aligned}
\mu' &= 12\mu, \quad E' = \frac{E}{1 - \nu^2}, \\
K' &= 4\left(\frac{2}{\pi}\right)^{1/2} K_{Ic}, \quad C' = 2C_L.
\end{aligned}
\tag{1}
$$

Here E' is the plane strain modulus, and μ' is the scaled fluid viscosity, while K' and C' the scaled fracture toughness and leak-off coefficient. These scaled quantities are introduced to keep equations uncluttered by numerical factors.

2.2.1. ELASTICITY

Given the assumptions that the rock is homogeneous and linear elastic, the equations relating the displacement discontinuity component and induced stress fields in the solid can be condensed into the following hypersingular integral equations Crouch and Starfield (1983); Hills et al. (1996):

$$
\begin{aligned}
\sigma_{iz}(x, y, z_k) &= \sum_{l=1}^{n_p} \int_{A_l(t)} C_{izj}(x - \chi, y - \eta, z_k - z_l) \\
&\times D_{j,l}(\chi, \eta) d\chi d\eta,
\end{aligned}
\tag{2}
$$

where $A_l(t)$ denotes the fracture footprint of lth fracture, $C_{izj}(x - \chi, y - \eta, z_k - z_l)$ represents the the izth stress component at point (x, y, z_k) due to a unit displacement discontinuity at point (χ, η, z_l) in the jth coordinate direction (the expressions for C_{izj} are omitted for brevity). The total stress field is a sum of the hydraulic fracture induced stress whose ij components are σ_{ij} and the geological stress with the ij components σ_{ij}^g. Since the fractures typically grow in planes that are perpendicular to the minimum principal stress, then $\sigma_{xz}^g(x, y) = \sigma_{yz}^g(x, y) = 0$. To include the effects of stress barriers, the zz component of the geological stress is assumed to vary according to

$$
\sigma_{zz}^g = \sigma_{zz}^0 + \Delta\sigma \mathcal{H}(y - \tfrac{1}{2}H) + \Delta\sigma \mathcal{H}(-y - \tfrac{1}{2}H),
\tag{3}
$$

where $\mathcal{H}$ denotes Heaviside step function, while H is the thickness of the reservoir layer. Since the fluid cannot sustain shear stresses, the boundary conditions at fracture surfaces are

$$
\sigma_{xz}(x, y, z_l) = 0, \quad \sigma_{yz}(x, y, z_l) = 0,
\tag{4}
$$

while the fluid pressure in lth fracture is calculated based on

$$
p_l(x, y) = \sigma_{zz}(x, y, z_l) + \sigma_{zz}^g(x, y),
\tag{5}
$$

where the expression for the geological stress σ_{zz}^g is given in (3).
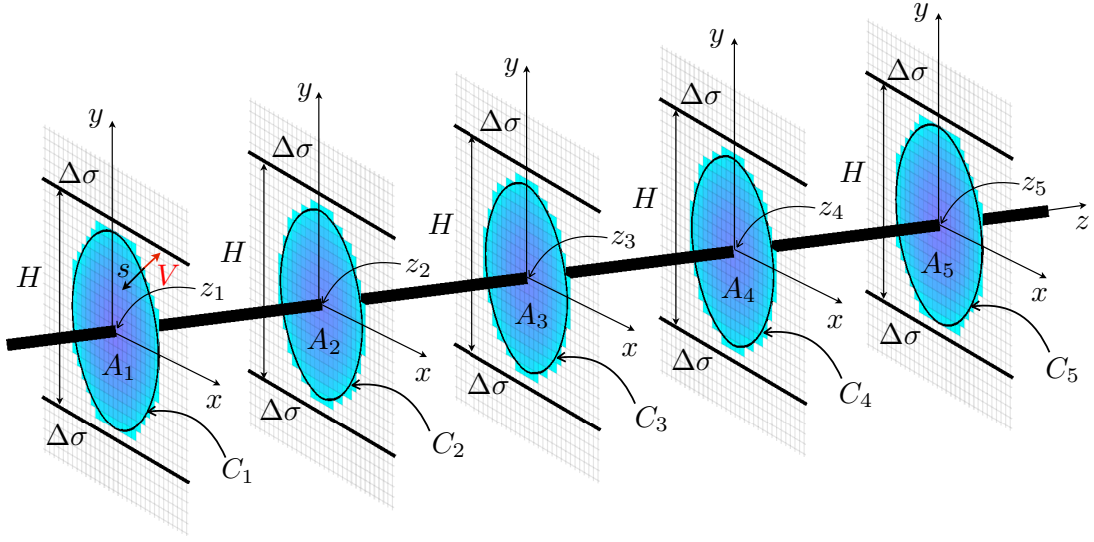
Figure 1: Schematics of simultaneously growing multiple parallel hydraulic fractures.

2.2.2. TURBULENT LUBRICATION THEORY

The continuity equation for each fracture is

$$\frac{\partial w_l}{\partial t} + \boldsymbol{\nabla} \cdot \mathbf{q}_l + \frac{C'}{\sqrt{t-t_{0,l}(x,y)}} = Q_l(t)\delta(x,y), \qquad (6)$$

where $\boldsymbol{\nabla} = (\partial/\partial x, \partial/\partial y)$, the last term on the left hand side captures the fluid leak-off according to the Carter's model, and $t_{0,l}(x,y)$ signifies time instant at which the fracture front of lth fracture was located at the point (x,y). Turbulent fluid low is incorporated using the phenomenological Darcy-Weisbach equation, which relates the pressure drop along the flow to the fluid velocity as

$$-\boldsymbol{\nabla}p_l = f_D(Re_l, \epsilon_l)\frac{\rho}{2}\frac{U_l^2}{D_l}\frac{\boldsymbol{U}_l}{U_l}, \quad Re_l = \frac{\rho U_l D_l}{\mu}, \quad \epsilon = \frac{r_l}{D_l}, \qquad (7)$$

where ρ is the mass density of the fluid, $\boldsymbol{U} = (U_x, U_y)$ is the average fluid velocity vector and $U = \sqrt{U_x^2 + U_y^2}$ is its magnitude, D is the hydraulic diameter of the channel, and the dimensionless friction factor f_D depends on the Reynolds number Re and the relative roughness ϵ is defined in terms of the absolute wall roughness r.

We adopt Churchill's (Churchill, 1977) empirical approximation for f_D that was derived for circular pipes, adapted by Dontsov (Dontsov, 2016) to flow geometries in hydraulic fractures with hydraulic diameter $D = 2w$, which has the following form:

$$f_D = \frac{96}{Re}\tilde{f}_D, \qquad \tilde{f}_D(Re, r) = \left(1 + (\tilde{A}+\tilde{B})^{-1.5}\right)^{1/12}, \quad (8)$$

where f_D has been scaled by the factor $\dfrac{96}{Re}$ associated with laminar flow to define $\tilde{f}_D$ and the remaining parameters are given by

$$\begin{aligned} \tilde{A} &= \left[\frac{8.511}{Re^{1/2}}f_0(Re, r)\right]^{16}, \qquad \tilde{B} = \left(\frac{2566}{Re}\right)^{24}, \\ Re &= \frac{24\rho U w}{\mu'}, \qquad r = \frac{\epsilon}{2w}. \end{aligned} \qquad (9)$$

where $f_0(Re, r) = \left|\log\left(\left(\frac{7}{Re}\right)^{0.9}+0.27r\right)\right|$. We note that (8) is able to capture laminar ($Re \lesssim 2000$), transition ($2000 \lesssim Re \lesssim 3000$), and turbulent ($Re \gtrsim 3000$) regimes.

Combining (7) and (8), the flux can be expressed in the form

$$\mathbf{q}_l = \boldsymbol{U}_l w_l = -\frac{w_l^3}{\mu' \tilde{f}_D(Re_l, r_l)}\boldsymbol{\nabla}p_l. \qquad (10)$$

We note that this expression for the flux is in the same form as that for the classic Poiseuille law for laminar flow in which the additional factor factor $\tilde{f}_D(Re_l, r_l) \geq 1$ automatically increases the the viscosity as the flow velocity increases into the turbulent regime. Laminar Poiseuille flow is obtained by setting $\tilde{f}_D(Re_l, r_l) = 1$ and when the effect of turbulence is important the factor $\tilde{f}_D(Re_l, r_l) > 1$.

Combining (10) and (6) yields the Reynolds equation for the lth fracture

$$\begin{aligned} \frac{\partial w_l}{\partial t} &= \frac{1}{\mu'}\boldsymbol{\nabla} \cdot \left(\frac{w_l^3}{\tilde{f}_D(Re_l, r_l)}\boldsymbol{\nabla}p_l\right) \\ &\quad - \frac{C'}{\sqrt{t-t_{0,l}(x,y)}} + Q_l(t)\delta(x,y), \qquad (11) \end{aligned}$$

Assuming no fluid-lag, the governing equation (11) applies within the whole fracture for all $l = 1...n_p$. The fluid fluxes that enter each of the fracture may be different, but the total flux in the wellbore is prescribed, so that

$$\sum_{l=1}^{n_p} Q_l(t) = Q_0(t), \qquad p_i(0,0,t) = p_j(0,0,t). \qquad (12)$$

Here the second equation states that the fluid pressure is the same along the whole wellbore (i.e. for every fracture), while $i = 1...n_p$, $j = 1...n_p$, and $i \neq j$.

2.2.3. BOUNDARY CONDITIONS AT THE MOVING FRONT

Due to the assumption that the fracture propagation is determined by LEFM, growth of the mode I crack can be described by Rice (1968):

$$\lim_{s \to 0} \frac{w_l}{s^{1/2}} = \frac{K'}{E'}, \qquad (13)$$

where s is the distance to the fracture front. Assuming that there is no lag a zero flux boundary condition Detournay and Peirce (2014) should be imposed at the fracture tip:

$$\lim_{s \to 0} w_l^3 \frac{\partial p_l}{\partial s} = 0. \qquad (14)$$

The evolution of the fracture front $C_l(t)$ (and the associated normal velocity V) is implicitly determined by the equations (2), (11), (13) and (14), which apply for all fractures $l = 1...n_p$.

2.2.4. LOCATING THE MOVING FRONT USING A MULTISCALE UNIVERSAL TIP ASYMPTOTIC SOLUTION

From the second equation in (9) we observe that the Reynolds number is proportional to the fracture width. Thus, as we approach the fracture tip, the Reynolds number decreases. In this study we assume the we are sufficiently close to the tip that the Reynolds number has been reduced sufficiently for the flow in the near-tip region to be considered laminar. Analysis of the near tip behavior of hydraulic fractures indicates that the validity region of the propagation condition (13) is often limited to the immediate vicinity of the tip (see e.g. Garagash et al. (2011)). Resolving the square root behaviour at the length scale at which it applies would require an extremely fine mesh, which is computationally prohibitive. To obtain accurate solutions on a relatively coarse mesh the propagation condition (13) can be replaced by an asymptotic solution w_a that has a much larger region of validity

$$w_l(s) \approx w_a(s), \qquad s = o(L), \qquad (15)$$

where L is the characteristic length of the fracture. The universal asymptotic solution w_a can be calculated by considering a semi-infinite hydraulic fracture that propagates steadily with a velocity V under plane strain elastic conditions Garagash et al. (2011); Peirce and Detournay (2008).

By considering a non-singular formulation Dontsov and Peirce (2015) of the steadily propagating semi-infinite hydraulic fracture problem it has been possible to express the asymptotic solution (15) in the following implicit form:

$$\frac{s^2 V \mu'}{E' w_a^3} = g_\delta \left(\frac{K' s^{1/2}}{E' w_a}, \frac{2 s^{1/2} C'}{w_a V^{1/2}} \right), \qquad (16)$$

where g_δ is relatively simple function that can be evaluated efficiently. This solution captures all the multiscale behavior associated with the competing processes of viscous dissipation, toughness energy release, and fluid leak-off, reduces to all the so-called vertex limiting solutions, and captures all possible transition regions, see Dontsov and Peirce (2015, 2017) for more details.

The role of the uniform asymptotic solution (16) in locating the fracture free boundary and capturing the multiscale behavior on a coarse mesh is two-fold. Firstly, given trial fracture widths w_l at selected sample points in the vicinity of the tips the corresponding distances s to the fracture tips are determined. Given this distance information the free boundary for the lth fracture is determined as the zero level set $T_l(x, y) = 0$ of the solution to the eikonal equation $|\nabla T_l| = 1$. Secondly, having established the location of the free boundary, the zeroth and first moments of the width defined in (16) are used to impose the multiscale asymptotic solutions in a weak sense. These are the two essential steps used by the so-called Implicit Level Set Algorithm

(ILSA) to locate the fracture free boundaries and to capture the multiscale mutiprocess solution on a relatively coarse mesh.
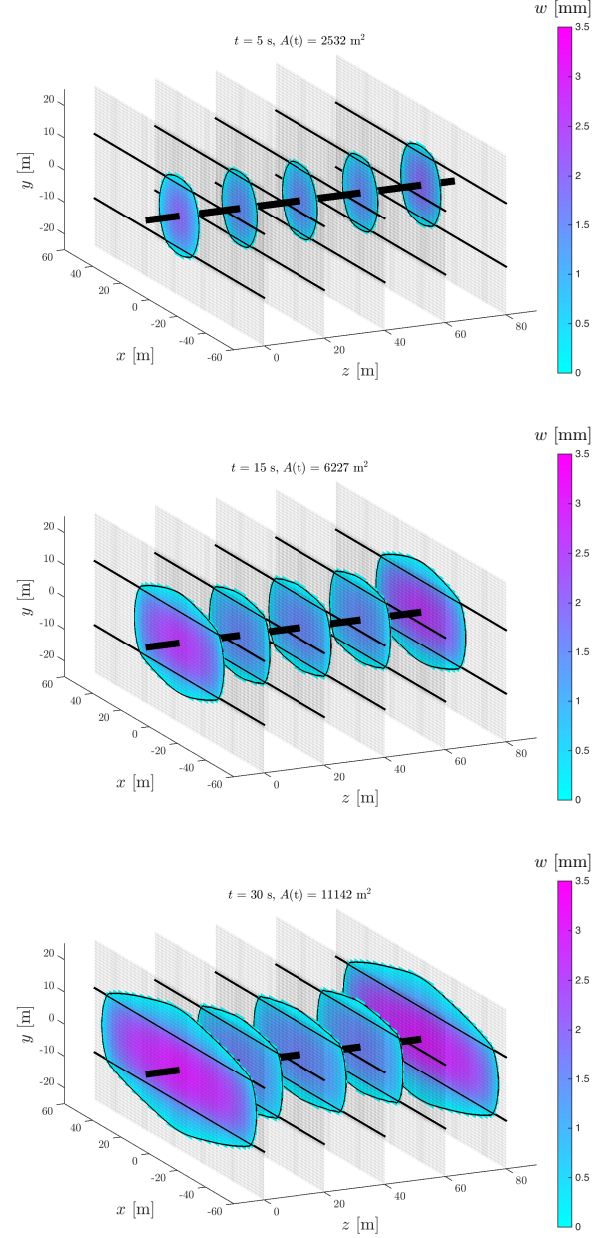

Figure 2: Results of the numerical simulations for the laminar case at times $t = 5$ s (top), $t = 15$ s (middle), and $t = 30$ s (bottom).

3. NUMERICAL RESULTS

In this section we provide results in which the ILSA scheme Peirce and Bunger (2014); Peirce (2015); Peirce and Detournay (2008); Dontsov and Peirce (2017) is used to obtain the numerical solution of (2)–(5), (11), (12) along with the propagation condition (15) that is implemented using the approximate solution (16). The following material parameters are used in the

examples:

$$
\begin{aligned}
E &= 9.5\,\text{GPa}, \quad \nu = 0.2, \quad K_{Ic} = 0.5\,\text{MPa·m}^{1/2}, \quad (17) \\
Q_0 &= 0.5\,\text{m}^3/\text{s}, \quad \mu = 0.002\,\text{Pa·s}, \quad C' = 0\,\text{m/s}^{1/2}, \\
H &= 20\,\text{m}, \quad \rho = 1000\,\text{kg/m}^3, \quad r = 10^{-4}\,\text{m}.
\end{aligned}
$$

In the case of laminar flow either we could use Poiseuille's law directly or enforce it by setting $\rho = 0$ in which case $Re = 0$ and $\tilde{f}_D(Re_l, r_l) = 1$.

The confining stresses in (3) are assumed to be

$$
\sigma_{zz}^0 = 7\,\text{MPa}, \qquad \Delta\sigma = 0.75\,\text{MPa}. \qquad (18)
$$

The spacing between perforations is selected to be uniform and equal to 20 m, i.e. $z_{k+1} - z_k = 20$ m for $k = 1...n_p - 1$. This study focuses on the case of five parallel fractures, i.e. $n_p = 5$.
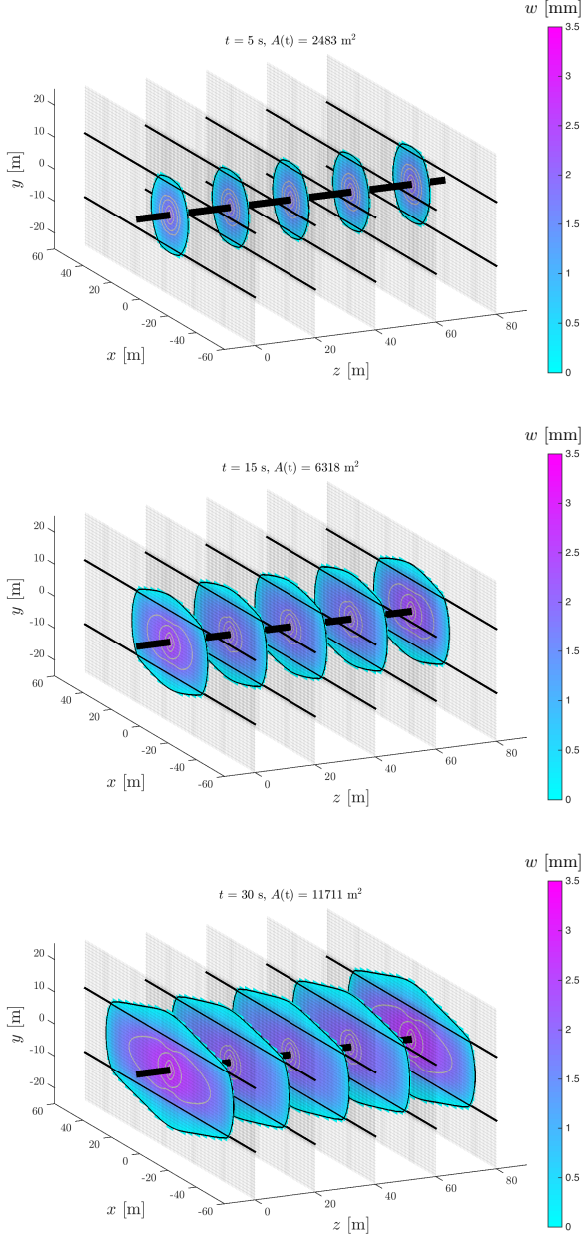

Figure 3: Results of the numerical simulations for the turbulent case at times $t = 5$ s (top), $t = 15$ s (middle), and $t = 30$ s (bottom). Grey lines indicate contour levels at which $\tilde{f}_D = \{1.1, 2, 4, 8\}$.

Fig. 2 shows the results of the numerical simulations at times $t = 5$ s (top), $t = 15$ s (middle), and $t = 30$ s (bottom) for the laminar case for which $\tilde{f}_D = 1$. Color filling is used to indicate the fracture width according to the colorbar. The fracture boundaries (footprints) are highlighted by solid black lines, the locations of the stress barriers are shown by thicker solid lines (at $y = 10$ m and $y = -10$ m), while the thickest black line passing through $x = 0$, $y = 0$ represents the wellbore. The total surface area, $A(t)$, of all five fractures at time t is shown on each picture. At $t = 5$ s all the fractures have entered the regions of higher confining stress and though the middle three fractures are slightly smaller than the outer two, there has not been significant stress shadowing by this stage. At time $t = 15$ s the effect of stress shadowing is noticeable, while by time $t = 30$ s the stress shadowing has resulted in outer fractures that have grown significantly compared to the inner three fractures.

Fig. 3 shows the results of the numerical simulations at times $t = 5$ s (top), $t = 15$ s (middle), and $t = 30$ s (bottom) using the turbulent flow model (10). As before color filling is used to indicate the fracture width, fracture boundaries (footprints) are highlighted by solid black lines, the locations of the stress barriers are shown by thicker solid lines (at $y = 10$ m and $y = -10$ m), and the thickest black line passing through $x = 0$, $y = 0$ represents the wellbore. The total surface area, $A(t)$, of all five fractures at time t is shown on each picture. Within each of the fractures contours of the viscosity factor $\tilde{f}_D$ are plotted by the grey lines at levels $\tilde{f}_D = \{1.1, 2, 4, 8\}$ that increase toward the wellbore. For the contour encompassing the largest region $\tilde{f}_D = 1.1$, which implies that the viscosity at all points along this curve has only increased by 10 %. Thus this outer contour can be regarded as the transition curve outside of which there is laminar flow and inside of which there is turbulent flow. From this figure it can be seen that the results are consistent with the assumption that close to the tip the flow is laminar - so that the universal asymptotic solution (15), which was derived for laminar flows, can be used in this situation. In addition, the fact that the flow within the fracture is part laminar and part turbulent emphasizes the need for a flow model that is able to capture not only the laminar and the turbulent regimes but also the transition form laminar to turbulent regimes. The contour $\tilde{f}_D = 2$, encapsulating the second largest region, indicates the points at which the viscosity is doubled due to the effect of turbulence. As is to be expected the contours of highest turbulence are clustered around the wellbore. At $t = 5$ s all the fractures have entered the regions of higher confining stress, however there has not been a noticeable stress shadow effect. The less pronounced stress shadowing when turbulent effects are included can also be seen from the solutions provided at later times. Indeed, comparing the laminar solutions from Fig. 2 to the turbulent solutions in Fig. 3 at corresponding times we observe that the turbulent solutions exhibit significantly less stress shadowing.

This reduction in stress shadowing can be explained by the significantly larger pressure drop at the wellbore for the turbulent case compared to the laminar case. This can be demonstrated by estimating the asymptotic behaviour of the pressure gradient field near the wellbore. Due to the point source represented by the δ-function, it can be shown that close to the well bore the flux behaves as $q \sim 1/r$. For laminar flow Poiseuille's law implies that $\partial p/\partial r \sim q \sim 1/r$. For turbulent flow near the wellbore consider the limit $Re \gg 1$ in (8) and (9) from which it follows that $\tilde{f}_D \sim Re$. Thus (10) implies that $\partial p/\partial r \sim q^2 \sim 1/r^2$. Because the near-wellbore pressure gradient in the turbulent case is more singular than that in the laminar

case, the turbulent pressure drop near the well-bore dominates the mutual stress interactions between the fractures in the array to a much greater extent than in the laminar case. Therefore, including the the effect of turbulence near the wellbore leads the model to predict significantly less stress shadowing than the laminar case.
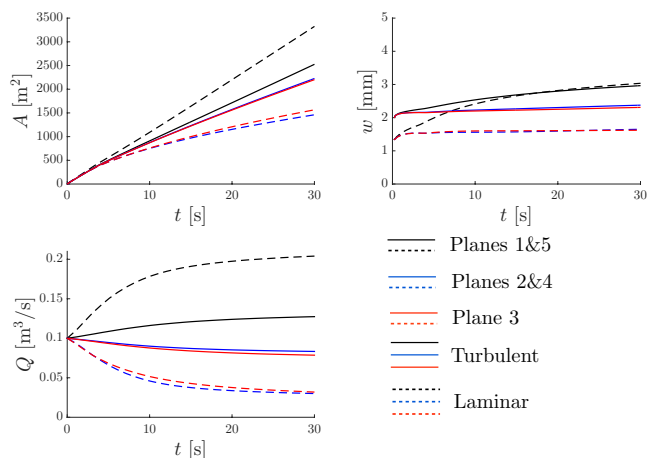

Figure 4: Time histories of fracture area (top left), width at the wellbore (top right), and wellbore flux (bottom left) for all the fracture planes for both the laminar and the turbulent cases.

To quantify the effect of the transition to turbulence on the propagation of multiple hydraulic fractures, Fig. 4 shows the time histories of the fracture area (top left), the fracture width at the wellbore, i.e. at $x = 0$ and $y = 0$ (top right), and the fluid flux (bottom left) for every fracture for both laminar and turbulent flows. Results for planes 1 and 5 (located at $z = 0$ and $z = 80$ m) are identical due to symmetry and are indicated by black lines. Results for planes 2 and 4 (located at $z = 20$ and $z = 60$ m) are also identical due to symmetry and are indicated by blue lines. Results for the middle plane 3 (located at $z = 40$ m) are indicated by red lines. The results for laminar flow are represented by dashed lines while those for turbulent flow are represented by solid lines. The laminar case shows significantly more stress shadowing as is evidenced by the significant differences in the areas, widths, and fluxes associated with plane 1 compared to planes 2 and 3. For the turbulent case the areas, widths, and fluxes for plane 1 are much closer to those for planes 2 and 3. While the fracture area time history for plane 1 (respectively planes 2 & 3) in the laminar case is significantly larger (respectively significantly smaller) than the turbulent case, the total fractured areas of all the planes in the array are slightly larger for the turbulent case than in the laminar case.

4. SUMMARY

The primary goal of this paper is to describe the implementation of a turbulent flow model into a multiplanar hydraulic fracture simulator that is able to capture laminar, turbulent, and the transition from laminar to turbulent regimes. Since the Reynolds number is proportional to the fracture width and therefore decays close to the fracture tip the flow reduces to the laminar regime near the fracture tip. This makes it possible to use the universal tip asymptotic solution that has been derived for laminar flows in order to establish a scheme to locate the fracture free boundary. The ILSA scheme Peirce and Bunger

(2014); Peirce (2015); Peirce and Detournay (2008); Dontsov and Peirce (2017) is used to implement the uniform asymptotic solution into the hydraulic fracturing simulator that is able to capture the multiscale behaviour associated with the competing processes of viscous dissipation, toughness energy release, and fluid leak-off.

The numerical experiments present results for five simultaneously propagating pseudo-3D-like fractures evolving in uniformly distributed planes.The laminar flow model yields a solution with significant stress shadowing as the fractures evolve whereas the the turbulent model for the same parameter set yields a solution with significantly less stress shadowing. The explanation for this difference stems from the much larger stress drop near the wellbore in the turbulent case to which the mutual stress interactions between the fractures (that are responsible for stress shadowing) are subdominant compared to the laminar case.

ACKNOWLEDGEMENTS

REFERENCES

Abou-Sayed, A.S., D.E. Andrews, and I.M. Buhidma. 1989. Evaluation of oily waste injection below the permafrost in prudhoe bay field. In *Proceedings of the California Regional Meetings, Bakersfield, CA, Society of Petroleum Engineers*, pages 129–142.

Brown, D. W. 2000. A hot dry rock geothermal energy concept utilizing supercritical co_2 instead of water. In *Proceedings of Twenty-Fifth Workshop on Geothermal Reservoir Engineering Stanford University, Stanford, California*.

Carter, E.D. 1957. Optimum fluid characteristics for fracture extension. In *Howard GC, Fast CR, editors. Drilling and production practices*, pages 261–270.

Churchill, S.W. 1977. Friction factor equation spans all fluid flow regimes. *Chemical Engineering*, 7:91–92.

Crouch, S.L., and A.M. Starfield. 1983. *Boundary Element Methods in Solid Mechanics*. George Allen and Unwin, London.

Daneshy, A. 2014. Fracture shadowing: Theory, applications and implications. In *Proceedings of the SPE Annual Technical Conference and Exhibition, SPE-170611-MS*.

Detournay, E., and A. Peirce. 2014. On the moving boundary conditions for a hydraulic fracture. *Int. J Eng. Sci.*, 84:147–155.

Dontsov, E., and A. Peirce. 2015. A non-singular integral equation formulation to analyze multiscale behaviour in semi-infinite hydraulic fractures. *J. Fluid. Mech.*, 781:R1.

Dontsov, E.V. 2016. Tip region of a hydraulic fracture driven by a laminar-to-turbulent fluid flow. *J. Fluid. Mech.*, 797:R2.

Dontsov, E.V., and A.P. Peirce. 2016. Implementing a universal tip asymptotic solution into an implicit level set algorithm (ILSA) for multiple parallel hydraulic fractures. In *In Proceedings 50th U.S. Rock Mechanics Symposium, Houston, TX, USA, ARMA-2016-268, Houston, TX*. American Rock Mechanics Association.

Dontsov, E.V., and A.P. Peirce. 2017. A multiscale implicit level set algorithm (ILSA) to model hydraulic fracture propagation incorporating combined viscous, toughness, and leak-off asymptotics. *Comput. Methods Appl. Mech. Engrg.*, 313: 53–84.

Economides, M.J., and K.G. Nolte, editors. 2000. *Reservoir Stimulation*. John Wiley & Sons, Chichester, UK, 3rd edition.

Garagash, D., and E. Detournay. 2000. The tip region of a fluid-driven fracture in an elastic medium. *J. Appl. Mech.*, 67:183–192.

Garagash, D.I., E. Detournay, and J.I. Adachi. 2011. Multiscale tip asymptotics in hydraulic fracture with leak-off. *J. Fluid Mech.*, 669:260–297.

Hills, D.A., P.A. Kelly, D.N. Dai, and A.M. Korsunsky. 1996. *Solution of crack problems, The Distributed Dislocation Technique, Solid Mechanics and its Applications*, volume 44. Kluwer Academic Publisher, Dordrecht.

Jeffrey, R.G., and K.W. Mills. 2000. Hydraulic fracturing applied to inducing longwall coal mine goaf falls. In *Pacific Rocks 2000, Balkema, Rotterdam*, pages 423–430.

Kresse, O., X. Weng, H. Gu, and R. Wu. 2013. Numerical modeling of hydraulic fracture interaction in complex naturally fractured formations. *Rock Mech. Rock Eng.*, 46:555–558.

Kumar, D., and A. Ghassemi. 2015. 3D simulation of multiple fracture propagation from horizontal wells. In *In Proceedings 49nd U.S. Rock Mechanics Symposium. San Francisco, CA, USA*.

Manchanda, R., E.C. Bryant, P. Bhardwaj, P. Cardiff, and M.M. Sharma. 2016. Strategies for effective stimulation of multiple perforation clusters in horizontal wells. In *Proceedings of the SPE Hydraulic Fracturing Technology Conference, SPE-179126-MS*.

McClure, M.W., and M.D. Zoback. 2013. Computational investigation of trends in initial shut-in pressure during multi-stage hydraulic stimulation in the barnett shale. In *In Proceedings 47nd U.S. Rock Mechanics Symposium. San Francisco, CA, USA*.

Olson, J.E. 2008. Multi-fracture propagation modeling: Applications to hydraulic fracturing in shales and tight gas sands. In *In Proceedings 42nd U.S. Rock Mechanics Symposium. San Francisco, CA, USA*.

Peirce, A., and E. Detournay. 2008. An implicit level set method for modeling hydraulically driven fractures. *Comput. Methods Appl. Mech. Engrg.*, 197:2858–2885.

Peirce, A.P. 2015. Modeling multi-scale processes in hydraulic fracture propagation using the implicit level set algorithm. *Comp. Meth. in Appl. Mech. and Eng.*, 283:881–908.

Peirce, A.P., and A.P. Bunger. 2014. Interference fracturing: Non-uniform distributions of perforation clusters that promote simultaneous growth of multiple hydraulic fractures. *SPE 172500*.

Rice, J.R. 1968. Mathematical analysis in the mechanics of fracture. In H. Liebowitz, editor, *Fracture: An Advanced Treatise*, volume II, chapter 3, pages 191–311. Academic Press, New York, NY.

Singh, I., and J.L. Miskimins. 2010. A numerical study of the effects of packer-induced stresses and stress shadowing on fracture initiation and stimulation of horizontal wells. In *Proceedings of the Canadian Unconventional Resources & International Petroleum Conference, CSUG/SPE 136856*.

Skomorowski, N., M.B. Dussealut, and R. Gracie. 2015. The use of multistage hydraulic fracture data to identify stress shadow effects. In *In Proceedings 49nd U.S. Rock Mechanics Symposium. San Francisco, CA, USA*.

Wu, K., J. Olson, M.T. Balhoff, and W. Yu. 2015. Numerical analysis for promoting uniform development of simultaneous multiple fracture propagation in horizontal wells. In *Proceedings of the SPE Annual Technical Conference and Exhibition, SPE-174869-MS*.